Supplementary Material

Coupled CFD-DEM Simulation of Seed Flow in Horizontal-Vertical Tube Transition

1. Discrete Element Method Implementation Details

Particle motions calculated within the Discrete Element Method (DEM) solver are governed by Newton's second law. The combination of contact and body forces acting on a particle is used to determine the motion of each particle. The Hertz contact model governs interactions between particles as well as geometric boundaries (i.e. seed-seed and seed-wall interactions). When particles are in contact, the reaction force is determined by separating it into two components normal and shear. After the calculations are completed, the sum of all forces and their components provide the updated force acting in the particles, which is used to calculate the particles movement in between each timestep. The following descriptions provide a general overview of the DEM solver calculations for mechanical forces in PFC3D [1].

The force components are subdivided further into Hertz forces and dashpot forces (energy dissipation). The Hertz normal force, F_n^h, is calculated as follows:

$$F_n^h = -h_n \left| g_c \right|^{1.5} \tag{S1}$$

where h_n and g_c are the Hertz coefficient and contact gap, respectively.

The Hertz coefficient is calculated as follows:

$$h_n = \frac{2G\sqrt{2\overline{R}}}{3(1-\nu)} \tag{S2}$$

where G, R, and ν are the shear modulus, effective contact radius, and Poisson's ratio, respectively. The Hertz coefficient acts as the stiffness of the system and provides a relationship between the amount of particle deformation and appropriate reaction forces associated with it.

The effective radius is calculated as follows:

$$\frac{1}{\overline{R}} = \frac{1}{2}\left(\frac{1}{R^{(1)}} + \frac{1}{R^{(2)}} \right) \tag{S3}$$

where the superscripts 1 and 2 refer to particle radius of piece 1 and 2, respectively. Since the present study has uniform particle sizes, the effective radius is equal to the assigned particle radius.

The shear force is assigned depending on weather the initial force is enough to overcome the friction between contacts (sliding). When the particle is not sliding the shear force can be calculated as:

$$F_s^* = \left(F_s^0 \right)_0 + k_s \Delta\delta_s \tag{S4}$$

where F_s^0, k_s, and $\Delta\delta_s$ are the shear force at the beginning of the timestep, the tangent shear stiffness, and the relative shear increment, respectively.

The shear increment is given by:

$$k_s = \frac{2(1-\nu)}{2-\nu}\alpha_h h_n \left(F_n^h\right)^{(\alpha_h-1)/\alpha_h} \tag{S5}$$

where α_h is an exponent that must be selected depending on the simulation. The value of 1.5 is recommended in literature [2] and is almost universally used in all DEM simulations involving granular material flow.

When the particle is sliding, the shear force due to friction can be calculated as:

$$F_s^{\mu} = \mu F_n^h \tag{S6}$$

where μ is the coefficient of friction between the two contacts.

Dashpot forces are used to represent energy dissipated during collisions. This is important to generate realistic behaviours as collisions in physical systems are not perfectly elastic.

The normal dashpot force is calculated as:

$$F_n^d = \frac{3(1-e_n^2)h_n\dot{\delta}_n^{1.5}\dot{\delta}_n}{4\dot{\delta}_n^{(-)}} \tag{S7}$$

where e_n, $\dot{\delta}_n$, and $\dot{\delta}_n^{(-)}$ are the target restitution coefficient, normal component of the translational velocity, and the normal impact velocity, respectively.

Calculations of fluid forces acting on the particles are explained in detail in the main text (section 2.2.3). Combining all forces, particle motion cab be calculated for each timestep. Once the force balance has been resolved, the particle translational motion is calculated through the following relationship:

$$F = m(\ddot{x} - g) \tag{S8}$$

where F, m, $\ddot{x}$, and g are the sum of all forces acting on the particle, the mass of the particle, the acceleration due to body forces, and acceleration due to gravity, respectively.

The half timestep velocity is used to determine the particle position at the end of the time step and it can be calculated as:

$$\dot{x}^{(t+\Delta t/2)} = \dot{x}^{(t)} + \frac{1}{2}\left(\frac{F^{(t)}}{m} + g\right)\Delta t \tag{S9}$$

where $\dot{x}$ is the particle velocity.

The half timestep velocity is used to determine the particle position at the end of the timestep through the following formula:

$$x^{(t+\Delta t)} = x^{(t)} + \dot{x}^{(t+\Delta t/2)}\Delta t \quad \text{(S10)}$$

where x is the particle position.

At the end of the timestep new forces are calculated, witch result in a new acceleration and a new velocity that are used as the new initial conditions.

The particle rotational motion is computed in a similar way, in this case the three principal moments of inertia are equal (spherical body and center of mass at the centroid). The equations describing this rotational motion are:

$$L = I\omega \quad \text{(S11)}$$

where L, I, and ω are the angular momentum, the inertia tensor, and angular velocity, respectively.

$$M = I\dot{\omega} + \omega L \quad \text{(S12)}$$

where M and $\dot{\omega}$ are the resultant moment (from forces acting in the body) and angular acceleration, respectively.

$$\omega^{(t+\Delta t/2)} = \omega^{(t)} + \frac{1}{2}\left(\frac{M^{(t)}}{I}\right)\Delta t \quad \text{(S13)}$$

Similar to translational velocities, the updated resulting moments are used to determine the updated angular acceleration and velocity.

2. Computational Fluid Dynamics Numerical Schemes

Numerical schemes options used for the Computational Fluid Dynamics (CFD) portion of the simulation are shown in supplementary Table S1.

Table S1. Computational Fluid Dynamics (CFD) numerical schemes for OpenFOAM Sub-dictionaries

Sub-dictionary	Entry	Selection/Value
ddtSchemes	default	steadyState[1]/Euler[2]
gradSchemes	default	cellMDLimited Gauss linear 0.5
divSchemes	default	none
	div(phi,U)	Gauss limitedLinearV 1
	div(phi,k), div(phi,epsilon)	Gauss limitedLinear 1
	div((nuEff*dev2(T(grad(U)))))	Gauss linear
laplacianSchemes	default	Gauss linear limited 0.777[3]
interpolationSchemes	default	linear
snGradSchemes	default	limited 0.777[3]

[1] simpleFOAM, [2] pisoFOAM, [3] based on mesh non-orthogonality between 60 and 70.

3. Computational Fluid Dynamics Mesh Size Determination

The CFD element length is recommended to be 3 times the particle diameter. In order to simulate green field peas with a diameter of 6.94 mm the recommended element length was approximately 21 mm. This

was determined based on a general rule of thumb for application of CFD-DEM under the coarse-grid method. However, the combination of low SLR and relatively high air velocities provided some flexibility. Preliminary simulations were used to determine the minimum element size that would not result in numerical instabilities (low porosities of less than 0.5%) during two-way coupling simulations. The minimum element size that could sustain a stable two-way coupled simulation at a seed rate of 0.07 kg/s was 10 mm. Three mesh files (coarse, moderate, and fine) with corresponding element sizes of 20, 10, and 5 mm were reviewed. This was done to determine if the 10 mm mesh size resulted in an appropriate level of discretization. Mesh discretization was evaluated by comparing velocity fields between meshes. Average velocity at the bend inlet and outlet areas was used in the discretization error calculations. Since the velocity data behaved in a monotonic fashion, calculation of grid convergence index (GCI) was performed as described by Roche [3,4]:

$$GCI_{[\,fine-grid\,]} = \frac{3|\varepsilon|}{r^{p}-1} \tag{S14}$$

$$GCI_{[coarse-grid\,]} = r^{p} \bullet GCI_{[\,fine-grid\,]} \tag{S15}$$

$$p = \ln\left(\frac{f_3 - f_2}{f_2 - f_1}\right) / \ln(r) \tag{S16}$$

$$r = \frac{h_2}{h_1} \tag{S17}$$

$$\varepsilon = \frac{f_2 - f_1}{f_1} \tag{S18}$$

where the ε is error estimator between two grids, r is the refinement factor between two grids, p is the formal order of accuracy of the algorithm, f is the grid numerical solution, h is the representative grid size, and the subscripts 3, 2, and 1 represent the values obtained from the coarse, moderate, and fine grid, respectively.

The GCI at a few areas were summarized in Table S2. The mesh refinement study revealed that grid size reductions resulted in lower GCI. However, the GCI results obtained from the meshes with 10 mm and 5 mm elements were relatively similar. Steady-state air velocity fields along the mid-plane show that the principal flow followed similar patterns with modest differences between moderate and fine meshes (Figure S2a and S2b). The moderate mesh size was confirmed as a good compromise between CFD solver accuracy and the ability to capture seed–airflow–wall interactions using the coarse-grid approach.

Table S2. Velocity measurements of 90-degree elbow steady-state airflow at bend inlet and bend outlet, rate of convergence (p), and Grid Convergence Index (GCI) for three mesh resolutions, with mesh length decreasing by factor of r=2 between meshes.

	Velocity at Bend inlet (m/s)				Grid Convergence Index (%)		
Inlet Velocity (m/s)	Coarse	Moderate	Fine	p	Coarse	Moderate	Fine
20	19.6	20.1	20.2	2.28	9.5	1.9	0.4
25	24.5	24.9	25.1	1.26	10.1	4.2	1.7
30	29.3	29.9	30.2	1.23	10.2	4.3	1.8
	Velocity at Bend outlet (m/s)				Grid Convergence Index (%)		
Inlet Velocity (m/s)	Coarse	Moderate	Fine	p	Coarse	Moderate	Fine
20	19.1	20.0	20.1	3.06	15.5	1.8	0.2
25	24.7	25.0	25.1	0.86	6.6	3.6	2.0
30	29.7	30.0	30.1	0.71	7.6	4.6	2.8

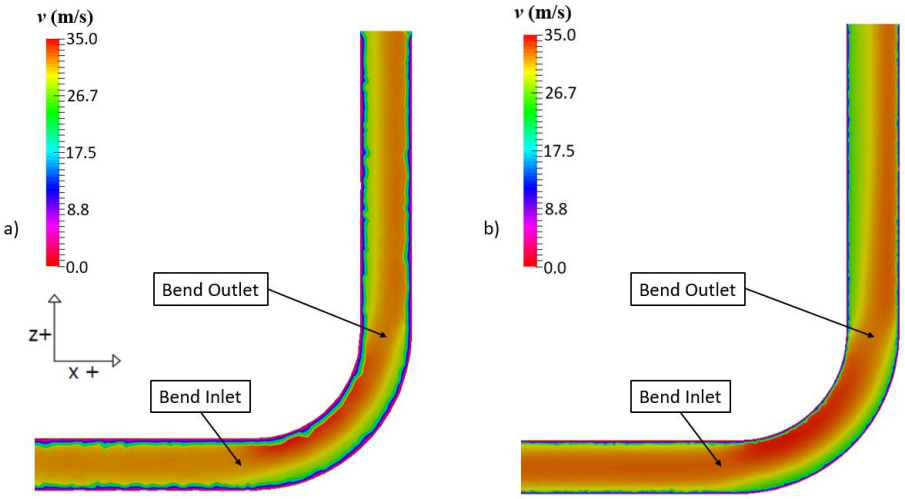

Figure S1. Steady-state air velocity (v) profile for 30 m/s inlet velocity at elbow mid-plane: a) Moderate mesh, b) Fine mesh

References

1. Itasca. PFC3D Particle Flow Code in 3 Dimensions, Verification Problems and Example Applications; Itasca Consulting Group, Inc.: Minneapolis, MN, USA, 2017.

2. Tsuji, Y.; Tanaka, T.; Ishida, T. Lagrangian Numerical Simulation of Plug Flow of Cohesionless Particles in a Horizontal Pipe. *Powder Technol.* **1992**, *71*, 239–250, doi:10.1016/0032-5910(92)88030-L.

3. Roache, P.J. Perspective: A Method for Uniform Reporting of Grid Refinement Studies. *J. Fluids Eng. Trans. ASME* **1994**, *116*, 405–413, doi:10.1115/1.2910291.

4. Roache, P.J. Quantification of Uncertainty in Computational Fluid Dynamics. *Annu. Rev. Fluid Mech.* **1997**, *29*, 123–160, doi:10.1146/annurev.fluid.29.1.123.